Unexpectedly Efficient Aging of Organic Aerosols Mediated by Autoxidation

Wen Zhang[1], Zixu Zhao[1,a], Chuanyang Shen[1], Haofei Zhang[1]*

[1]Department of Chemistry, University of California, Riverside, California 92507, USA

[a]Present address: Department of Environmental Sciences, Policy, and Management, University of California, Berkeley, California 94720, USA

*Corresponding Author. Email: haofei.zhang@ucr.edu

Abstract

Multiphase oxidative aging is a ubiquitous process for atmospheric organic aerosols (OA). But its kinetics was often found to be slow in previous laboratory flow tube studies where high hydroxyl radical concentrations ([•OH]) were used. In this study, we performed heterogeneous oxidation experiments of several model OA systems under varied aging timescales and gas-phase [•OH]. Our results suggest that OA heterogeneous oxidation may be 2–3 orders of magnitude faster when [•OH] is decreased from typical laboratory flow tube conditions to atmospheric levels. Direct laboratory mass spectrometry measurements coupled with kinetic simulations suggest that an intermolecular autoxidation mechanism mediated by particle-phase peroxy radicals greatly accelerates OA oxidation, with enhanced formation of organic hydroperoxides, alcohols, and fragmentation products. With autoxidation, we estimate that the OA oxidation timescale in the atmosphere may be from less than a day to several days. Thus, OA oxidative aging can have greater atmospheric impacts than previously expected. Furthermore, our findings reveal the nature of heterogeneous aerosol oxidation chemistry in the atmosphere and help improve the understanding and prediction of atmospheric OA aging and composition evolution.

Keywords: Heterogeneous oxidation, Hydroxyl radicals, Peroxy radicals, Chain propagation, Organic hydroperoxides.

Synopsis: Condensed-phase intermolecular autoxidation largely accelerates organic aerosol aging under atmospheric oxidant concentrations and impacts aerosol compositions.

TOC:

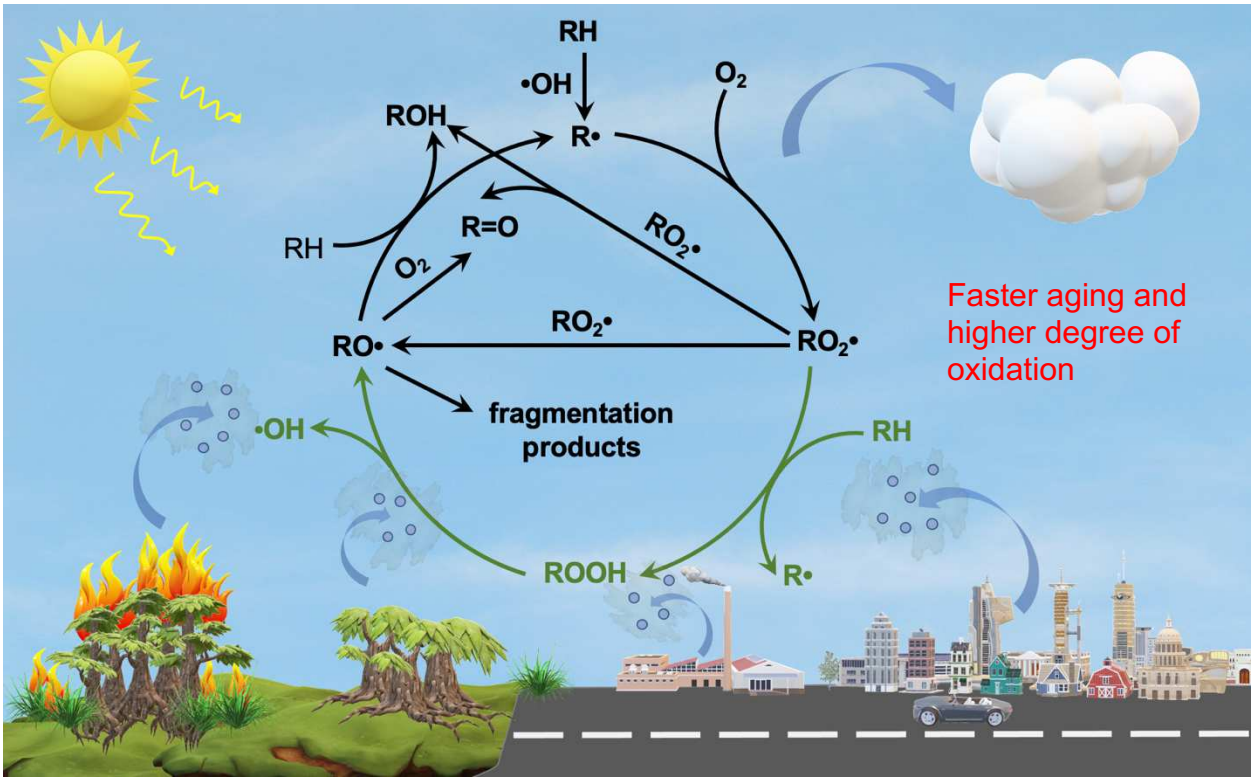
RH
•OH
O2
ROH
R•
R=O
RH
O2
RO2•
RO2•
RO•
RO2•
Faster aging and higher degree of oxidation
fragmentation products
•OH
RH
ROOH
R•

Introduction

Organic aerosols (OA) are ubiquitously present in the Earth's atmosphere and greatly contribute to fine particulate matter.[1, 2] The chemical composition and properties of atmospheric OA can significantly impact air quality, climate, and human health.[3, 4] Despite the immense ubiquity of OA and the oxidizing nature of the atmosphere, the OA reactivity through heterogeneous oxidation by gaseous oxidants such as hydroxyl radicals (•OH) has often been considered a slow process,[5-12] in comparison to the timescales of other important atmospheric processes and the overall aerosol lifetime.

The universal metric to quantify the heterogeneous oxidation kinetics is the effective reactive uptake coefficient of •OH (γ_{eff}), which describes the probability of •OH-particle collision leading to oxidation events:[7]

$$\gamma_{\text{eff}} = \frac{4k\rho N_A V}{\bar{c}MA} \qquad (1)$$

where k is the second-order degradation rate constant of an OA surrogate, ρ is the particle density, N_A is Avogadro's number, $\bar{c}$ is the mean thermal velocity of •OH, M is the molecular weight of the OA surrogate, V is the particle volume, and A is the particle surface area. Previous studies have often reported γ_{eff} in the range of 0.01–1.0,[5, 8-11, 13, 14] with the smaller γ_{eff} values often observed for more viscous OA due to that oxidation is confined at the particle surface region which the inside materials cannot efficiently diffuse to. The kinetic information expressed in γ_{eff} could also allow for estimation of the OA oxidation timescales by:[15]

$$\tau_{ox} = \frac{1}{k[\cdot OH]} = \frac{2d_p\rho N_A}{3\gamma_{\text{eff}}\bar{c}M[\cdot OH]} \qquad (2)$$

where d_p is the particle diameter. Thus, the γ_{eff} value of 0.01–1.0 translates to oxidation timescales up to several years. These significantly longer timescales than the typical aerosol lifetime in the

atmosphere (~ 10 days[16]) suggests that heterogenous oxidation of OA in the atmosphere is less important in affecting air quality and the climate compared to some of the commonly focused processes such as secondary OA formation which usually has a timescale of only a few hours to a day. Further, OA mass loss during heterogeneous oxidation within relevant timescale was found to be minimal, suggesting that it is not an efficient aerosol removal process.[8] However, these long-standing views were derived from previous laboratory studies using •OH concentrations 3–5 orders of magnitude higher than atmospheric concentrations (i.e., [•OH] ~ 10^9–10^{11} molecules cm^{-3}) to offset the short oxidation time (τ ~ 1 min or less) in flow tube reactors (FTR),[6, 7, 9-11, 13, 17] such that one can interpret OA oxidation under relevant atmospheric conditions, termed as "•OH exposure" (= [•OH] × τ).

Several prior studies have attempted to investigate the heterogeneous oxidation kinetics under lower [•OH] using FTR,[15, 18] continuous flow stirred tank reactors (CFSTR),[19] or environmental chambers.[20] A summary of the scarce kinetic measurements from these studies (**Figure S1**) implies that lower [•OH] could enhance γ_{eff} to varied extent (greater enhancement for oxidized OA), but large uncertainties from distinct experimental conditions impede accurate interpretations. In most of these studies, such [•OH]-dependent γ_{eff} was suggested to be caused by physical processes, including: (1) slower •OH reaction than the •OH adsorption at the gas-particle interface (i.e., the Langmuir-Hinshelwood mechanism),[15] (2) the diffusion limitation of organic molecules to the interface for •OH reaction,[20] or (3) O_3 (an •OH precursor) shielding the particle interface.[18] In contrast, Richards-Henderson et al. examined the chemical role of nitric oxide in increasing γ_{eff} via a chain propagation mechanism.[19] However, this mechanism is only relevant for highly polluted environment. It remains unclear whether [•OH]-dependent γ_{eff} may be explained by a generalized chemical mechanism relevant for typical atmospheric conditions.

Here, we probe the •OH-initiated heterogeneous oxidation of a few common OA model systems in a custom-designed CFSTR.[19, 21-23] Experiments were conducted under a large range of [•OH] (5×10^6–1×10^9 molecules cm^{-3}) to bring the OA aging conditions from typical laboratory [•OH] closer to ambient levels. The chosen OA surrogates (adipic acid, succinic acid, citric acid, and 3-methylglutaric acid) are highly oxidized compounds (O/C ratio ~ 0.7–1.2) containing multiple carboxylic acid functional groups. They all have been used in prior research to represent the oxygenated and viscous nature of generic OA in the atmosphere.[2, 10, 11, 13, 24-26] In these experiments, the particle diffusion coefficients (D_{org}, 10^{-8}–10^{-13} cm^2 s^{-1}) and mixing timescales (10^{-3}–10^2 s) are also representative of typical aerosol phase state in the lower troposphere.[26] Their degradation upon heterogeneous •OH-oxidation was monitored in real-time using a thermal desorption iodide-adduct chemical ionization mass spectrometer (TD-CIMS) to provide accurate kinetic measurements.[27, 28] The comprehensive OA oxidation products were measured by the TD-CIMS and an ion mobility spectrometry time-of-flight mass spectrometer (IMS-MS)[24, 27, 29-31] which provides additional isomer-resolved capability. Complementary FTR experiments were also performed following similar procedures as in previous studies.[27, 30] This allows for direct comparisons of the heterogeneous oxidation kinetics and products between the CFSTR and FTR experiments. In addition, a multilayer reaction-diffusion kinetic model was developed to simulate and interpret the experimental results.[27]

Materials and Methods

Experimental setup

All experiments were performed at 22 °C and varied water activity (a_w of 35–70%). A customized CFSTR (volume ~ 250 L)[31, 32] was used in this work with the setup shown in **Figure S2**. Here, the CFSTR was operated in the "semi-batch" mode under room temperature.[21] Before each experiment, the CFSTR was flushed overnight with clean dry air, supplied by a zero-air generator (Aadco Instrument, Inc.). At the beginning of each experiment, the CFSTR background was monitored to ensure that aerosol particles were not present. Polydisperse organic aerosols (OA) of selected model compounds were generated into the CFSTR using a constant output aerosol atomizer (TSI, Inc.). The OA injection was stopped when targeted OA mass concentration was reached (~ 2000–3000 μg m^{-3}). The high OA mass loading is necessary to allow sufficient detection of OA composition by several techniques and eliminate evaporation of parent OA during experiments. After OA injection, the clean air injection was adjusted to a total flow of 1.5 L min^{-1}. Two different a_w levels were studied for the OA model compounds: 0.36 ± 0.01 and 0.67 ± 0.03. For adipic acid and succinic acid, the injected OA through the dryer effloresced the particles and a_w levels do not change their phase state and D_{org}. But for citric acid that does not have an efflorescence point, different a_w levels lead to different amount of water in the OA and hence affect the phase state and D_{org}.[11, 33, 34] The 3-methylglutaric acid OA was only studied under a_w = 0.36. In all the CFSTR experiments, the mean surface-weighted particle diameters for adipic acid, succinic acid, citric acid, and 3-methylglutaric acid were 210 ± 50 nm, 420 ± 120 nm, 290 ± 15 nm, and 221 ± 17 nm, respectively. After the OA injection, a one-time injection of a VOC tracer (either acetic acid or propionic acid) was made to reach a VOC concentration of 1–2 ppm. After both the OA and VOC tracer have been injected, they were allowed to undergo dilution (caused by the continuous flow) and wall loss in the CFSTR (**Figure S3**). Then, either O_3 or H_2O_2 was continuously injected into the CFSTR. With the mercury UV lamps on (λ = 254 nm), this injection

initiated the in-situ generation of •OH radicals.[27, 30] By changing the injection concentration of O_3 or H_2O_2, the [•OH] was controlled. During the •OH-initiated oxidation, the total flow rate and a_w were maintained the same as the "dilution and wall loss only" period. Therefore, the changes in the decay rates of both the OA and VOC tracer were caused by oxidation. The oxidation was maintained for 1–2 hours. To compare results obtained from the CFSTR experiments, auxiliary FTR experiments were performed in parallel with the CFSTR studies. The setup for the FTR is the same as our previous work.[24, 27, 29, 30] The injection system and the kinetic measurements are the same as for the CFSTR experiments. In both reactors, NO_x is below our detection limit (< 0.5 ppb) and is expected to play a negligible role in the OA aging experiments.

Instrumentation

The schematics of the instrumentation are shown in **Figure S2**. The OA particle size distribution and number concentration were analyzed by a scanning electrical mobility spectrometer and mixing condensation particle counter (SEMS and MCPC, Brechtel Inc.). A high-sensitivity proton-transfer-reaction mass spectrometer (PTR-MS, Ionicon Analytik Inc.) was used to measure the decay of the VOC tracers at 0.3 L min^{-1} in some experiments.[35] The OA composition was measured in real time by an iodide-adduct time-of-flight CIMS (Aerodyne Research Inc., m/Δm ~ 4000) with a TD tube following a charcoal denuder to remove volatile gases.[27, 28, 31] The desorption temperature was set to 90 – 160 °C for different OA systems to vaporize most of the particle mass (> 90%) and almost all the parent OA species. For the experiments in which the PTR-MS was unavailable, the VOC tracers were also monitored by the CIMS, where a separate gas sampling line was added bypassing the TD unit. The oxidation of 3-methylglutaric acid and adipic acid OA was used as the model system for the offline chemical

composition analysis and comparison between the CFSTR and FTR results. The oxidized OA particles were collected using a sequential spot sampler (Aerosol Devices Inc.) downstream of a charcoal denuder. The collected OA samples were immediately extracted by acetonitrile and infused into an electrospray ionization (ESI) IMS-MS (Aerodyne Research Inc.) in the negative ion mode. The IMS-MS measurements could provide isomer-resolved characterization by separating ionized molecules with their structure-dependent collisional cross sections.[36, 37] More details were described in our prior studies.[24, 27, 30, 32] Finally, a UV-visible spectrophotometer (Agilent Inc., 8453) was used for total ROOH quantification (see Supporting Information, SI for details).

Calculations of the heterogeneous oxidation kinetics and timescales

By comparing the decay rates of the parent OA compound and the VOC tracer before and after the oxidation (**Figure S3**), the [•OH] in the CFSTR and the second-order oxidation rate constants (k) of parent OA compound through heterogenous OH oxidation were determined. Specifically, the •OH oxidation rate constants of acetic acid and propionic acid ($k_{VOC+•OH}$) were known from the literature (6.6×10^{-13} cm^3 molecule^{-1} s^{-1} and 1.64×10^{-12} cm^3 molecule^{-1} s^{-1}, respectively).[38, 39] Thus, the [•OH] can be calculated by:

$$[\cdot OH] = \frac{k_{VOC,ox} - k_{VOC,DL}}{k_{VOC+\cdot OH}} \qquad (3)$$

where $k_{VOC,ox}$ and $k_{VOC,DL}$ are the first-order VOC decay rates during the oxidation period and the dilution-wall loss period, respectively. Then, the second-order oxidation rate constants (k) of parent OA compound through heterogenous •OH oxidation was calculated by:

$$k = \frac{k_{OA,ox} - k_{OA,DL}}{[\cdot OH]} \qquad (4)$$

where $k_{OA,ox}$ and $k_{OA,DL}$ are the first-order parent OA decay rates during the oxidation period and the dilution-wall loss period, respectively. The four first-order decay rates ($k_{VOC,ox}$, $k_{VOC,DL}$, $k_{OA,ox}$, and $k_{OA,DL}$) were obtained from the PTR-MS or TD-CIMS measurements. The high-frequency measurements made by the two instruments allow for high confidence decay rates, and hence reliable estimates of k. The k values were then used to calculate the effective uptake coefficient (γ_{eff}) shown in Equation (1).[7] Therefore, the relationships between the γ_{eff} and [$^{\bullet}$OH] can be obtained. The oxidation timescales are hence estimated by Equation (2).[15]

The reaction-diffusion multilayer kinetic model

To explain the experimental observation, a reaction-diffusion multilayer kinetic model was developed, as described in our previous work[27] and is essentially a similar representation to several other models that simulates heterogeneous OA oxidation processes.[40-42] The model constructs a multi-compartment rectangular prism to approximate the OA particle (**Figure S4**). The area of the square surface of the prism is set to be the same as the spherical OA aerosol in the experiments and the height of the rectangular prism is $d_p/6$ to maintain the same surface-to-volume ratio of the spherical aerosol and hence preserves the relevant scaling between surface and bulk processes. The thickness of each compartment is set to 0.5 nm, which was suggested to be a good representation of semisolid and solid aerosol particles.[42] Each compartment is assumed to be a well-mixed volume. The model includes (1) the adsorption, desorption, and reactions of $^{\bullet}$OH and $HO_2^{\bullet}$ at the outermost (i.e., surface) compartment of the OA particles, (2) organic radical-centered and multi-generational reactions in each compartment, and (3) diffusions of all the species molecules between compartments and evaporation of the relatively volatile products from the

surface compartment to gas phase. The FACSIMILE software was used to perform the simulations.[27] See SI for more details.

Results and Discussion

Heterogeneous oxidation kinetics

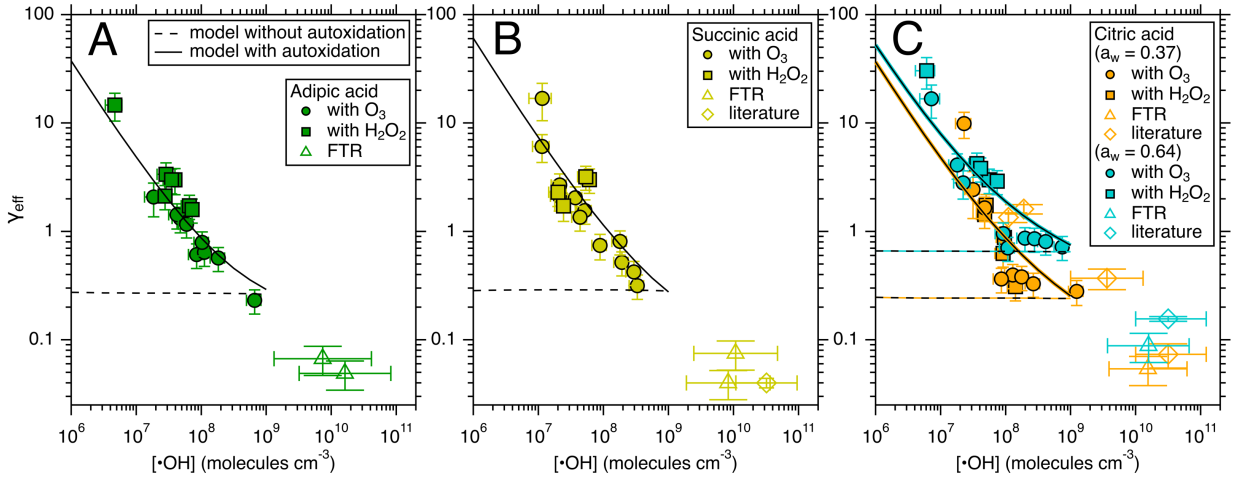

Figure 1. The γ_{eff} – [•OH] relationship for OA surrogate systems. (A) adipic acid, (B) succinic acid, and (C) citric acid, under various experimental conditions (see figure legend). For succinic acid (B) and citric acid (C), measurements from a few prior studies are also shown.[10, 11, 13, 20] For citric acid, experiments were performed under two different a_w conditions, resulting in different D_{org} values (see SI). Model simulations with and without the consideration of autoxidation are shown with the experimental data. Similar γ_{eff} – [•OH] trend obtained from three 3-methylglutaric acid experiments (**Figure S5**) is in general consistency with the results shown here.

As shown in **Figure 1**, the measured γ_{eff} exhibits striking enhancement as [•OH] decreases from ~ 1×10^9 to ~ 5×10^6 molecules cm^{-3} for all the studied OA systems. As [•OH] approaches

atmospheric levels (10^6 –10^7 molecules cm^{-3}), the γ_{eff} values are 2–3 orders of magnitude higher than those obtained from the high-[•OH] FTR experiments performed in this work and in prior studies. It is also worth noting that in the citric acid system, where varied a_w was studied, higher a_w and hence faster diffusion in the particles led to larger γ_{eff} under [•OH] > ~ 10^8 molecules cm^{-3} (**Figure 1C**), agreeing with prior work.[11, 13, 43] However, the difference appears to diminish as [•OH] further drops, implying that particle-phase diffusion may not be a key limitation for OA multiphase oxidative aging under ambient conditions. These kinetic results suggest that OA heterogeneous oxidation in the atmosphere may have a much shorter timescale than previously expected. For example, for a 500-nm diameter particle under [•OH] of 10^6 molecules cm^{-3}, γ_{eff} of 10 indicates an oxidation timescale of ~ 2.3 days, compared to 231 days when γ_{eff} is 0.1. These kinetic results are qualitatively consistent with prior studies (**Figure S1**), but contain more data points with smaller uncertainties, and hence are directly comparable to obtain the [•OH]-dependent γ_{eff}.

To investigate the cause of the [•OH]-dependent γ_{eff}, we used a multilayer reaction-diffusion kinetic model (see SI for details). The model explicitly considers the adsorption and desorption of •OH at the gas-particle interface and the diffusion and reactions at the particle surface and in the bulk.[27, 40, 44] The main reaction mechanism in the model is shown in **Figure 2** (top part), where self-reaction of peroxy radical (RO_2•) plays a central role: •OH oxidizes a parent OA molecule (RH) through H-abstraction and produces an alkyl radical (R•); RO_2• is subsequently formed following oxygen addition; the RO_2• + RO_2• self-reaction then produce an alcohol-carbonyl pair (ROH and R=O), known as the Russell mechanism, or two alkoxy radicals (RO•);[5, 45] the RO• may decompose to smaller oxidized products or undergo chain propagation reactions (i.e., RO• + RH),[19] forming an alcohol product and a new RO_2•. The mechanism may occur at multiple generations, forming multifunctional products.[7, 24] For instance, both ROH and R=O can

be further oxidized to form $R(OH)_2$ (diol), $R(=O)_2$ (dicarbonyl), and R(=O)OH (hydroxycarbonyl). This mechanism has been widely accepted to explain the major heterogeneous OA oxidation products observed in prior research. However, the kinetic model with this mechanism fails to simulate the increased γ_{eff} with reduced [$^{\bullet}$OH] (**Figure 1**), indicating that the traditional $RO_2^{\bullet}$ + $RO_2^{\bullet}$ dominant chemistry cannot explain the observations. Moreover, the results also suggest that the previously attributed Langmuir-Hinshelwood mechanism[15] and particle-phase diffusion limitation[20] do not explain the increased γ_{eff} with reduced [$^{\bullet}$OH] under the studied conditions of [$^{\bullet}$OH] and particle D_{org}, because these processes are already implemented in the kinetic model. The model performance is consistent with other models developed in previous studies which also considered these processes.[14, 44] The O_3 shielding mechanism[18] can also be ruled out as we observed similar γ_{eff}–[$^{\bullet}$OH] behavior by using H_2O_2 as the $^{\bullet}$OH precursor instead of O_3 (**Figure 1**). Furthermore, the previously proposed RO$^{\bullet}$-driven chain propagation reactions could only slightly enhance γ_{eff},[19] and is independent of [$^{\bullet}$OH] (**Figure S6**). Therefore, the [$^{\bullet}$OH]-dependent γ_{eff} suggests that a previously unrecognized mechanism is needed to explain the high γ_{eff} under low [$^{\bullet}$OH].

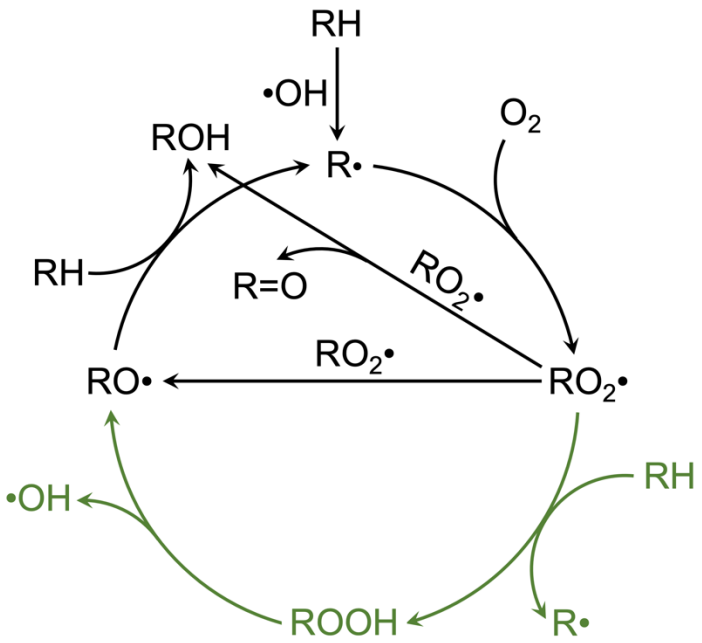

Figure 2. The •OH-initiated heterogeneous oxidation mechanism of organic aerosols in the atmosphere. The top part of the scheme (in black) illustrates the previous mechanistic understanding, and the bottom part (in green) shows the autoxidation mechanism proposed in this work.

Oxidation products highlight the formation of organic hydroperoxides

To elucidate the unrecognized mechanism, we further examined the oxidation products (**Figure 3**). Consistent with the above-mentioned reaction scheme, the most abundant products observed from these experiments by the TD-CIMS are R=O and ROH from the $RO_2^\bullet$ + $RO_2^\bullet$ self-reaction. Interestingly, another major product with two additional oxygens than RH ("RH+2O") was also observed in some of the studied OA systems. We determine this product to be the organic hydroperoxide (ROOH) for the reasons discussed below. Although the same chemical formula could be the second-generation products $R(OH)_2$, the absence of the other two expected concurrent second-generation products (i.e., R(=O)OH and $R(=O)_2$) from the TD-CIMS measurements ruled

this out (**Figure 3A–B**). In contrast, these expected second-generation products were all observed in the high-[•OH] FTR experiments. Additionally, the "RH+2O" signal appears almost simultaneously with the onset of •OH oxidation, while a second-generation product is usually indicated by delayed formation.[7] To further confirm its identity, the IMS-MS was used to compare the oxidation products between experiments under different [•OH] on the isomer-resolved level and with higher sensitivity. In this comparison (**Figure 4**), adipic acid oxidation under very different [•OH] produced identical isomer distributions and abundances for both R=O and ROH (**Figure 4 A, B, D, and E**). In contrast, "RH+2O" exhibits very different isomer distributions between the two [•OH] conditions, with a unique and dominant isomer present only under lower [•OH] (**Figure 4 C vs. F**), providing unambiguous evidence for ROOH formation. Moreover, auxiliary total hydroperoxide analysis also supports the formation of ROOH under low [•OH] in the CFSTR (**Figure S7**). In **Figure 3C–D**, we present the signal-based fractions of R=O and "RH+2O" among the three major products as a function of [•OH] in the adipic acid system, where all three products were detected. The results, compared with measurements from the high-[•OH] FTR experiments, clearly show that the formation of R=O is inhibited while "RH+2O" (mostly ROOH) is enhanced under low [•OH]. On the contrary, most of "RH+2O" detected under high [•OH] in the FTR are $R(OH)_2$ (**Figure 4F**). This [•OH]-dependent OA composition also explains the contradiction between this work and prior studies which reported no evidence of ROOH formation,[7, 46] as prior studies used high [•OH] to investigate OA oxidative aging. Finally, to test whether the ROOH formation is formed from the $RO_2^\bullet$ + $HO_2^\bullet$ reactions, we incorporated $HO_2^\bullet$ uptake and subsequent $RO_2^\bullet$ + $HO_2^\bullet$ reactions into the model using known kinetic parameters.[47, 48] However, the results suggest that this process plays a negligible role in γ_{eff} prediction and is unlikely to produce sufficient ROOH under the studied conditions (see SI). In support of this,

282 [•HO_2] is expected to be higher with increased [•OH] and thus, ROOH formed from RO_2• + HO_2•
283 should also increase with [•OH], which is opposite to the observed ROOH trend (**Figure 3D**). It
284 should also be pointed out that during thermal desorption in TD-CIMS, decomposition of the
285 products, especially ROOH, cannot be ruled out. However, thermal decomposition should not
286 affect the ROOH trends shown in **Figure 3** and may indicate that the formation of ROOH is even
287 more important.

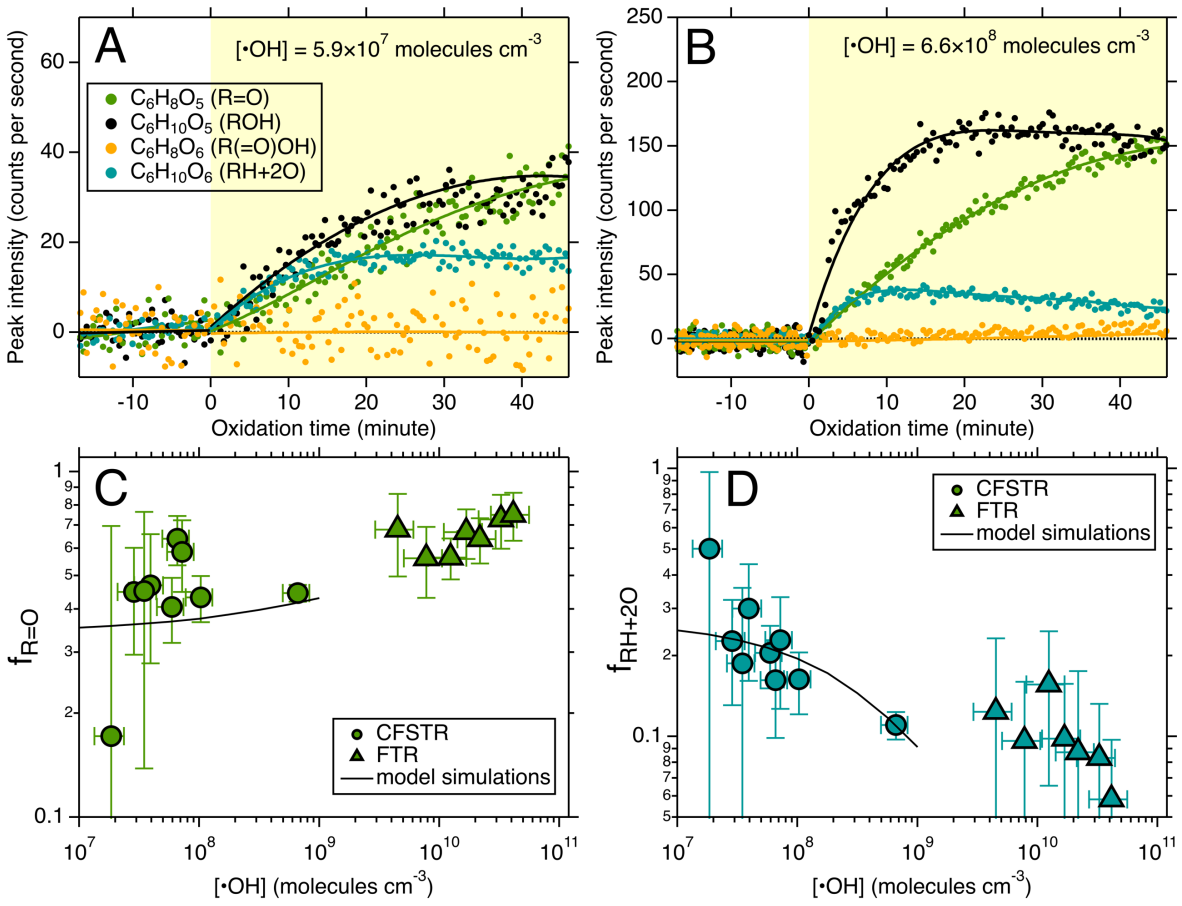

288

289 **Figure 3.** Major products from adipic acid OA oxidation. (A – B) TD-CIMS time-series of the
290 three major first-generation products (i.e., R=O, ROH, and "RH+2O") for two adipic acids
291 oxidation CFSTR experiments under different [•OH]. For comparison, one of the second-
292 generation products (R(=O)OH) is shown. The other second-generation product, $R(=O)_2$, is also
293 absent as R(=O)OH and hence is not shown. The light-yellow shades suggest the oxidation periods;

the fitted curves are to guide the eye. (C – D) The fractions of R=O and "RH+2O" in the first-generation products from adipic acid oxidation experiments. The error bars represent the measurement standard deviation, and the curves are model results. The model simulations with autooxidation only considers the ROOH as $R(OH)_2$ is not explicitly represented in the model. The simulations show consistent trends with the measurements. The similar time series results for 3-methylglutaric acid are shown in **Figure S8**.

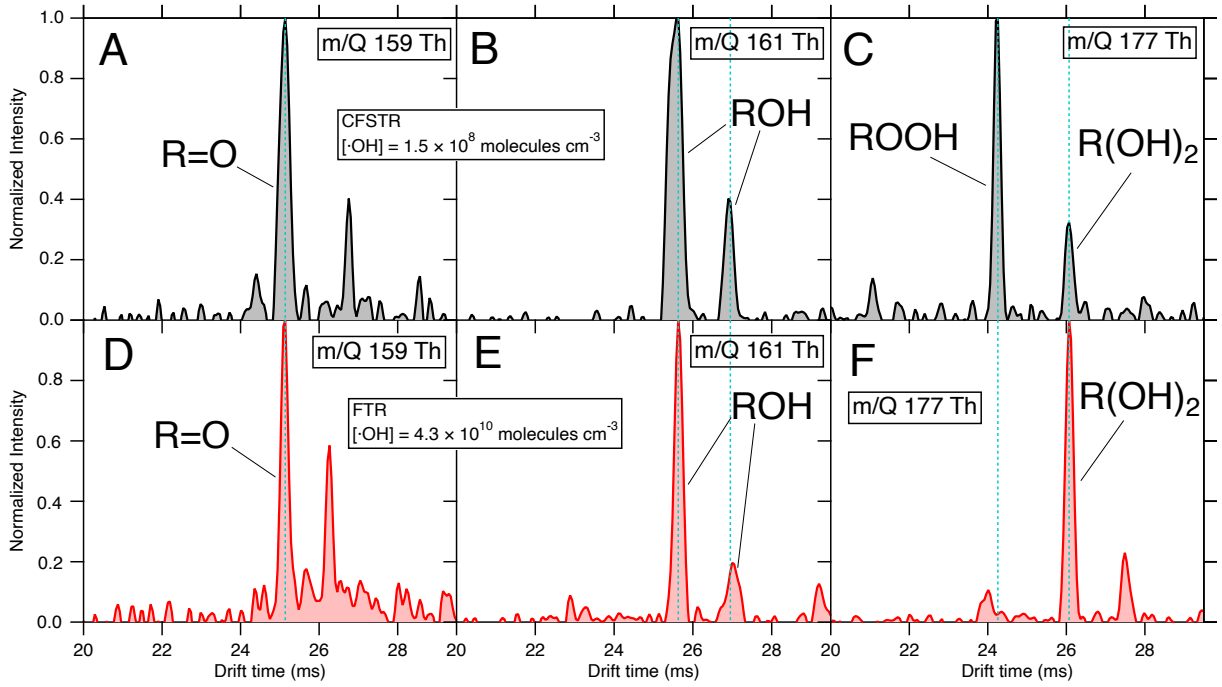

Figure 4. Comparison of R=O, ROH, and "RH+2O" on the isomeric level between CFSTR (A – C) and FTR (D – F) experiments by the IMS-MS. The same drift time peaks suggest identical structures. The unique peak in (C) at 24.2 ms in m/Q 177 Th, specific only to the low-[•OH] CFSTR experiment, is identified as the ROOH.

Autoxidation as the key aging mechanism

Through relating the enhancement of both γ_{eff} and ROOH formation under low [$^{\bullet}$OH], we propose a chain reaction mechanism between $RO_2^{\bullet}$ and RH, leading to the formation of ROOH and regenerating $RO_2^{\bullet}$ in the presence of O_2 (**Figure 2**, bottom part). The formed ROOH may decompose into $RO^{\bullet}$ and $^{\bullet}$OH, both of which could abstract H from RH in the condensed phase. This $RO_2^{\bullet}$-mediated mechanism thus sustains the other chain reaction ($RO^{\bullet}$ + RH) and creates additional secondary pathways to consume RH and form ROH and $RO_2^{\bullet}$, further increasing γ_{eff}. Under high [$^{\bullet}$OH], the large $^{\bullet}$OH flux at the particle surface leads to the substantial formation of $RO_2^{\bullet}$, thus favoring the $RO_2^{\bullet}$ + $RO_2^{\bullet}$ self-reaction. With lower [$^{\bullet}$OH], the interfacial and particle-phase [$RO_2^{\bullet}$] also decreases, allowing for the competing $RO_2^{\bullet}$ + RH reaction to become nonnegligible. As a result, the formation of ROOH is promoted and that of R(=O) is inhibited with low [$^{\bullet}$OH]; in contrast, ROH may be formed in both processes. This mechanism has been known for decades in biochemistry and polymer chemistry for lipids and rubbers (also known as "autoxidation"),[49-51] but for the first time here, this mechanism is reported in aerosol chemistry. It should be noted that this intermolecular autoxidation mechanism is essentially different from the unimolecular autoxidation chemistry (i.e., intramolecular H-shift followed by O_2 addition) for gas phase $RO_2^{\bullet}$.[52] Here, we demonstrate that the intermolecular autoxidation mechanism in the condensed phase exhibits a unique [$^{\bullet}$OH]-dependent behavior in aerosol chemistry, suggesting that the OA heterogeneous oxidation results obtained in the past decades may not accurately describe the processes occurring in the real atmosphere.

Following the proposal of the autoxidation mechanism, we implemented it into the kinetic model to aid the interpretation of the experimental results. The $RO_2^{\bullet}$ + RH reaction rate constant is estimated to be on the order of 10^{-6} times slower than that for $RO^{\bullet}$ + RH.[53] The ROOH decomposition rate may vary significantly, likely owing to the stability and reactivity of the ROOH.

Although some studies showed that ROOH can be stable in room temperature for as long as 24 hours,[54, 55] ROOH in atmospheric OA were more often found to be rather labile, especially for the highly functionalized molecules, with first-order decomposition rate ranging from 3×10^{-5} s^{-1} to ~ 2×10^{-3} s^{-1}.[56-59] Further, little in known regarding the detailed ROOH decomposition mechanism and products. Unimolecular decomposition via breaking the weak O–O bond to form $RO^{\bullet}$ and $^{\bullet}OH$ was suggested as a possible reaction at ambient temperature for peroxides with O/C ratios at 0.5 or higher.[56] In addition, bimolecular reactions were also suggested, such as the Baeyer-Villiger reaction and Korcek mechanism.[57, 60] But these bimolecular mechanisms do not directly produce free radicals, hence cannot propagate the chain reactions shown in **Figure 2**. The lack of detailed kinetic and mechanistic understanding leads to great challenges to explicitly incorporate the ROOH chemistry into the kinetic model. Therefore, we lumped the possible ROOH unimolecular[56] and bimolecular[57] decomposition pathways as a single pseudo first-order decomposition reaction forming $RO^{\bullet}$ + $^{\bullet}OH$ with a first-order decomposition rate constant and a tunable yield (see SI for model details).

Despite the simplification, this model reasonably reflects the chain propagating nature of the autoxidation mechanism. To capture the observed γ_{eff} – [$^{\bullet}OH$] relationship over the entire studied [$^{\bullet}OH$] range, optimization suggests that the model needs to constrain the formation rate of $RO^{\bullet}$ + $^{\bullet}OH$ from ROOH decomposition at 1×10^{-5}–1×10^{-4} s^{-1}, while keeping the $RO_2^{\bullet}$ + RH reaction rate constant in a reasonable range (i.e., 5–20×10^{-21} cm^3 $molecules^{-1}$ s^{-1}) for all the studied OA systems. Here, the formation rate of $RO^{\bullet}$ + $^{\bullet}OH$ is a combination of ROOH decomposition rate and the branching ratio of $RO^{\bullet}$ + $^{\bullet}OH$. For example, if all the ROOH decomposition forms $RO^{\bullet}$ + $^{\bullet}OH$, the decomposition rate is the same as the formation rate of $RO^{\bullet}$ + $^{\bullet}OH$; while if only 10% of ROOH decomposes to $RO^{\bullet}$ + $^{\bullet}OH$, the overall ROOH decomposition rate needs to be

approximately one order of magnitude higher, which is still within the range of previously reported ROOH decomposition rate constant mentioned above.[56-59] Model simulations of the γ_{eff} – [•OH] relationship using the autoxidation mechanism agree nicely with the measurements (**Figure 1**), suggesting that autoxidation in the condensed phase can indeed greatly accelerate OA aging under atmospherically relevant [•OH]. It should be noted that the good model-observation agreement does not require a certain unique set of parameters. Rather, with a given formation rate of RO• + •OH in the above-mentioned range, a coupled RO_2• + RH reaction rate constant can be determined to result in a similarly good agreement as shown in **Figure 1**. Furthermore, it is remarkable that the model results also agree with the trends of [•OH]-dependent fractions of R=O and "RH+2O" (**Figure 3C–D**), further supporting the autoxidation mechanism. Lastly, to test whether other radical-involved chemical processes might affect or contribute to the enhanced OA degradation, unimolecular H-shift isomerization for RO_2• and RO• were considered in the kinetic model. This unimolecular process has been shown to play important roles in the gas phase,[52, 61, 62] but our model simulations suggest that they are not fast enough at typical reaction rate constants to compete with the autoxidation mechanism and play a very minor role in OA aging kinetics (see SI).

The kinetic model further suggests that autoxidation-involved reactions (i.e., RH + RO_2•, RH + RO•, and RH + •OH from ROOH decomposition) could account for > 95% of total RH consumption under atmospheric [•OH] (**Figure S9**). This means that the collision of gas-phase •OH with OA particles plays more of an initiator role, rather than acting as the dominant oxidant of OA under atmospheric conditions. This also implies that once the oxidation is triggered, autoxidation may proceed even in the dark. Since most of the OA molecules are not oxidized directly by the •OH from gas-phase adsorption under low [•OH], the OA oxidation is no longer confined to the interfacial region of the particles. Consistently, model results suggest that the OA

oxidation could occur throughout the entire particles under atmospherically relevant [•OH], contrary to the dominant interfacial oxidation under much higher [•OH] for all the examined OA systems (**Figure S10**). Thus, for particles that are viscous and do not rapidly mix, autoxidation could make a big difference. Beyond the D_{org} range for the studied OA, the simulations indicate that even for more viscous OA particle across the semi-solid and solid ranges, the OA oxidation events could still spread throughout the particles in about an hour under atmospheric [•OH] (**Figure S11**). These simulations highlight that the autoxidation mechanism leads to highly efficient OA aging by allowing the oxidation to occur in the particle bulk and bypassing diffusion limitations, hence, making the viscous particles more homogeneous during oxidation.

Overall aerosol composition influenced by autoxidation

Finally, we investigated how intermolecular autoxidation may impact the entire OA composition. For this purpose, we focus on the 3-methylglutaric acid system which is more readily oxidized and can form diverse oxidation products.[24] The observed oxidation products ($C_{1-6}H_{2-10}O_{3-8}$) by the IMS-MS were employed to calculate the intensity-based elemental ratios, averaged carbon number (n_C), and fraction of fragmentation products in the particle phase under different oxidation conditions (**Figure 5**). As the Van Krevelen diagram shown in **Figure 5A**, the FTR experiments with the highest [•OH] (> ~ 2×10^{10} molecules cm^{-3}) exhibit the steepest H/C – O/C trajectory, with a slope ~ -0.91, indicative of a mechanism that forms similar amounts of carbonyls and alcohols (consistent with the Russell mechanism). In comparison, the lower [•OH] CFSTR experiments all had shallower H/C – O/C trajectories, with slopes of -0.65 – -0.69 under [•OH] < ~ 2×10^8 molecules cm^{-3} and -0.82 under [•OH] ~ 2×10^9 molecules cm^{-3}. The slope shift as a function of [•OH] suggests that low [•OH] favors the formation of alcohols and hydroperoxides

over carbonyls, consistent with the autoxidation mechanism. This mechanistic difference was also supported by comparing the major functionalization products: higher abundance of alcohols and hydroperoxides were observed in the CFSTR than the FTR (**Figure S12**) and higher ratios of the "RH+2O" signals over the other two major second-generation products were found under lower [$^{\bullet}$OH] (**Figure S13**). As a result of the enhanced hydroperoxides by autoxidation, the low-[$^{\bullet}$OH] CFSTR experiments reached comparable carbon oxidation state with the high-[$^{\bullet}$OH] FTR experiments, but at much lower $^{\bullet}$OH exposure (**Figure S14**). It is also evident that under [$^{\bullet}$OH] > ~ 2×10^9 molecules cm^{-3} (in both reactors), the fraction of fragmentation products increases and n_C decreases exponentially with $^{\bullet}$OH exposure (**Figure 5B**), consistent with prior understanding that fragmentation is increasingly important after the functionalization products are further oxidized. However, under lower [$^{\bullet}$OH] (< ~ 2×10^8 molecules cm^{-3}), an appreciable fraction of the total measured products are fragmentation products (20–30% based on peak intensities, **Figure 5B**), even with very low $^{\bullet}$OH exposure (i.e., < 10^{11} molecules cm^{-3} s). We suggest that this is because the enhanced autoxidation under low [$^{\bullet}$OH] promotes RO$^{\bullet}$ formation through ROOH decomposition and hence increase fragmentation even with low $^{\bullet}$OH exposure. These results suggest that autoxidation could provide a new pathway to rapidly produce small, oxidized compounds which could evaporate to the gas phase and contribute to important atmospheric processes such as secondary OA formation.

Overall, the chemical composition of oxidized OA provides observation-based support to the autoxidation mechanism and ROOH decomposition pathways. Specifically, the increased formation of alcohol and fragmentation products under lower [$^{\bullet}$OH] strongly supports the ROOH unimolecular decomposition to RO$^{\bullet}$ + $^{\bullet}$OH;[56] the enhanced alcohol formation may also be partly

due to the Baeyer-Villiger reactions.[60] Therefore, it is likely that both ROOH processes take place to promote autoxidation and explain the measurements.

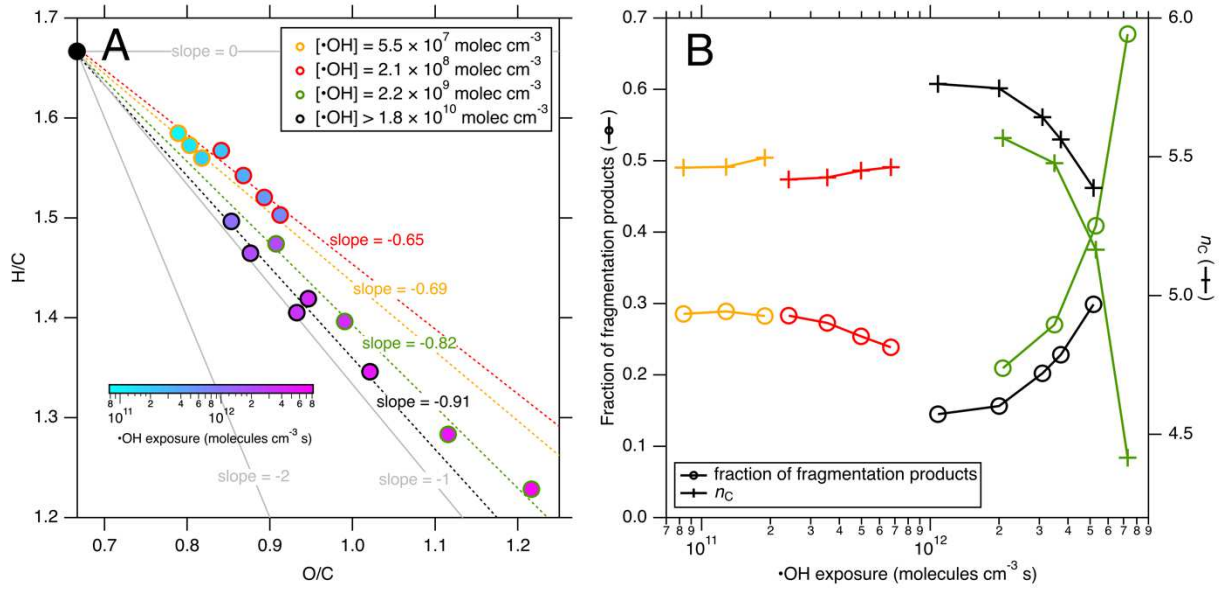

Figure 5. Chemical composition of oxidized 3-methylglutaric acid OA. (A) The Van Krevelen diagram for four 3-methylglutaric acid oxidation experiments. The experiment with the highest [•OH] was performed in the FTR and the other three lower-[•OH] experiments were performed in the CFSTR. The linear fits with slopes are shown with the data; the color scale indicates the •OH exposure for each data point. (B) The fraction of fragmentation products (left axis) and n_C (right axis) as a function of •OH exposure for the same 3-methylglutaric acid oxidation experiments as in (A).

Atmospheric Implications

In this work, we report strong and direct evidence for an intermolecular autoxidation mechanism in heterogeneous oxidative aging of OA. Although only a few highly oxidized OA surrogates were examined, its chemical nature is rather nonspecific.[50, 51, 53] Previous work showed a somewhat similar γ_{eff} – [•OH] dependence, but to a lesser degree for less oxidized OA

surrogates.[7, 19, 63] This could be caused by different kinetic parameters in the autoxidation mechanism (**Figure S15**). We show that autoxidation may occur at much faster rates than the other particle-phase $RO_2^•$ pathways under atmospherically relevant [$^•$OH] (e.g., $RO_2^•$ reactions with $RO_2^•$ and $HO_2^•$) and significantly boost OA oxidation. Through autoxidation, OA oxidative aging in the atmosphere may proceed on timescales from less than a day to several days, much more rapidly than prior laboratory results have suggested. This result opens up new avenues for heterogeneous OA oxidation to play key roles in various atmospheric processes. Although the laboratory studies showed clear evidence for enhanced OA aging kinetics and the formation of ROOH, ROH, and fragmentation products, the autoxidation-involved kinetic parameters have large uncertainties. This is mainly caused by: (1) the RH + $RO_2^•$ reaction kinetics have been less studied for system relevant to atmospheric OA species;[53] and (2) the ROOH decomposition rate constant and mechanism are largely varied with chemical structures.[56-59] Therefore, the corresponding kinetic model is constrained within the wide ranges of reported values to our best knowledge. Thus, future studies are needed to help better determine the key parameters for more accurate prediction of multiphase OA aging kinetics.

In the atmosphere, many OA processes could occur simultaneous with aging (e.g., secondary aerosol formation, new particle formation and growth, aqueous-phase reactions, evaporation, etc.); thus, direct field evidence to support such rapid OA oxidation is unavailable. However, the autoxidation-mediated fast OA aging reported in this work should be considered in the interpretation of field measurements. Another surprising outcome of our findings is that the gas-phase $^•$OH is only an initiator of OA aging, rather than the main oxidant, implying that OA oxidative aging may efficiently take place even under dark conditions (e.g., nighttime or in indoor environments). Additionally, substantial ROOH may be present in the oxidized OA particles as

reactive oxygen species, which are well known to result in health effects.[64] We also suggest that autoxidation can lead to OA oxidation throughout the entire aerosol particle even for highly viscous OA, rather than confined at the gas-particle interface, as previously understood. Lastly, we show that autoxidation may have an extending influence on the entire OA particle composition during oxidative aging. It will increase the oxygenation of OA efficiently and facilitate fragmentation chemistry. The rapid and enhanced oxygenation of aerosol particles through this mechanism may result in increased cloud formation, leading to larger indirect climate effects. Overall, the autoxidation mechanism reported here unveils the nature of heterogeneous aerosol oxidation chemistry and highlights the need to rethink aerosol aging processes in the real atmosphere.

Associated Contents

Supporting Information

Additional experimental details of peroxide measurements, kinetic model simulations and sensitivity tests, and supplementary figures of measurements and results.

Author Information

Corresponding Authors

E-mail address: haofei.zhang@ucr.edu (H. Zhang).

Notes

The authors declare no competing financial interest.

Acknowledgements

This work is supported by the U.S. National Science Foundation (CHE-2002413).

485

References

1. Zhang, Q.; Jimenez, J. L.; Canagaratna, M. R.; Allan, J. D.; Coe, H.; Ulbrich, I.; Alfarra, M. R.; Takami, A.; Middlebrook, A. M.; Sun, Y. L.; Dzepina, K.; Dunlea, E.; Docherty, K.; DeCarlo, P. F.; Salcedo, D.; Onasch, T.; Jayne, J. T.; Miyoshi, T.; Shimono, A.; Hatakeyama, S.; Takegawa, N.; Kondo, Y.; Schneider, J.; Drewnick, F.; Borrmann, S.; Weimer, S.; Demerjian, K.; Williams, P.; Bower, K.; Bahreini, R.; Cottrell, L.; Griffin, R. J.; Rautiainen, J.; Sun, J. Y.; Zhang, Y. M.; Worsnop, D. R., Ubiquity and dominance of oxygenated species in organic aerosols in anthropogenically-influenced Northern Hemisphere midlatitudes. *Geophysical Research Letters* **2007,** *34*, L13801.
2. Jimenez, J. L.; Canagaratna, M. R.; Donahue, N. M.; Prevot, A. S. H.; Zhang, Q.; Kroll, J. H.; DeCarlo, P. F.; Allan, J. D.; Coe, H.; Ng, N. L.; Aiken, A. C.; Docherty, K. S.; Ulbrich, I. M.; Grieshop, A. P.; Robinson, A. L.; Duplissy, J.; Smith, J. D.; Wilson, K. R.; Lanz, V. A.; Hueglin, C.; Sun, Y. L.; Tian, J.; Laaksonen, A.; Raatikainen, T.; Rautiainen, J.; Vaattovaara, P.; Ehn, M.; Kulmala, M.; Tomlinson, J. M.; Collins, D. R.; Cubison, M. J.; Dunlea, E. J.; Huffman, J. A.; Onasch, T. B.; Alfarra, M. R.; Williams, P. I.; Bower, K.; Kondo, Y.; Schneider, J.; Drewnick, F.; Borrmann, S.; Weimer, S.; Demerjian, K.; Salcedo, D.; Cottrell, L.; Griffin, R.; Takami, A.; Miyoshi, T.; Hatakeyama, S.; Shimono, A.; Sun, J. Y.; Zhang, Y. M.; Dzepina, K.; Kimmel, J. R.; Sueper, D.; Jayne, J. T.; Herndon, S. C.; Trimborn, A. M.; Williams, L. R.; Wood, E. C.; Middlebrook, A. M.; Kolb, C. E.; Baltensperger, U.; Worsnop, D. R., Evolution of Organic Aerosols in the Atmosphere. In *Science*, Science: 2009; Vol. 326:5959, s. 1525-1529.
3. Boucher, O.; Randall, D.; Artaxo, P.; Bretherton, C.; Feingold, C.; Forster, P.; Kerminen, V.-M.; Kondo, Y.; Liao, H.; Lohmann, U.; Rasch, P.; Satheesh, S. K.; Sherwood, S.; Stevens, B.; Zhang, X.-Y. *Clouds and Aerosols*; IPCC: 2013; p 657.
4. Dockery, D. W.; Pope, C. A.; Xu, X.; Spengler, J. D.; Ware, J. H.; Fay, M. E.; Ferris, B. G.; Speizer, F. E., An Association between Air Pollution and Mortality in Six U.S. Cities. *N. Engl. J. Med.* **1993,** *329* (24), 1753-1759.
5. George, I. J.; Abbatt, J. P. D., Heterogeneous oxidation of atmospheric aerosol particles by gas-phase radicals. *Nature Chemistry* **2010,** *2* (9), 713-722.
6. George, I. J.; Vlasenko, A.; Slowik, J. G.; Broekhuizen, K.; Abbatt, J. P. D., Heterogeneous oxidation of saturated organic aerosols by hydroxyl radicals: uptake kinetics, condensed-phase products, and particle size change. *Atmos. Chem. Phys.* **2007,** *7* (16), 4187-4201.
7. Smith, J. D.; Kroll, J. H.; Cappa, C. D.; Che, D. L.; Liu, C. L.; Ahmed, M.; Leone, S. R.; Worsnop, D. R.; Wilson, K. R., The heterogeneous reaction of hydroxyl radicals with sub-micron squalane particles: a model system for understanding the oxidative aging of ambient aerosols. *Atmos. Chem. Phys.* **2009,** *9* (9), 3209-3222.
8. George, I. J.; Abbatt, J. P. D., Chemical evolution of secondary organic aerosol from OH-initiated heterogeneous oxidation. *Atmos. Chem. Phys.* **2010,** *10* (12), 5551-5563.
9. Kroll, J. H.; Lim, C. Y.; Kessler, S. H.; Wilson, K. R., Heterogeneous Oxidation of Atmospheric Organic Aerosol: Kinetics of Changes to the Amount and Oxidation State of Particle-Phase Organic Carbon. *J. Phys. Chem. A* **2015,** *119* (44), 10767-10783.
10. Kessler, S. H.; Nah, T.; Daumit, K. E.; Smith, J. D.; Leone, S. R.; Kolb, C. E.; Worsnop, D. R.; Wilson, K. R.; Kroll, J. H., OH-Initiated Heterogeneous Aging of Highly Oxidized Organic Aerosol. *J. Phys. Chem. A* **2012,** *116* (24), 6358-6365.
11. Davies, J. F.; Wilson, K. R., Nanoscale interfacial gradients formed by the reactive uptake of OH radicals onto viscous aerosol surfaces. *Chemical Science* **2015,** *6* (12), 7020-7027.

12. Hearn, J. D.; Renbaum, L. H.; Wang, X.; Smith, G. D., Kinetics and products from reaction of Cl radicals with dioctyl sebacate (DOS) particles in O2: a model for radical-initiated oxidation of organic aerosols. *Phys. Chem. Chem. Phys.* **2007,** *9* (34), 4803-4813.
13. Chan, M. N.; Zhang, H.; Goldstein, A. H.; Wilson, K. R., Role of Water and Phase in the Heterogeneous Oxidation of Solid and Aqueous Succinic Acid Aerosol by Hydroxyl Radicals. *J. Phys. Chem. C* **2014,** *118* (50), 28978-28992.
14. Arangio, A. M.; Slade, J. H.; Berkemeier, T.; Pöschl, U.; Knopf, D. A.; Shiraiwa, M., Multiphase Chemical Kinetics of OH Radical Uptake by Molecular Organic Markers of Biomass Burning Aerosols: Humidity and Temperature Dependence, Surface Reaction, and Bulk Diffusion. *J. Phys. Chem. A* **2015,** *119* (19), 4533-4544.
15. Slade, J. H.; Knopf, D. A., Heterogeneous OH oxidation of biomass burning organic aerosol surrogate compounds: assessment of volatilisation products and the role of OH concentration on the reactive uptake kinetics. *Phys. Chem. Chem. Phys.* **2013,** *15* (16), 5898-5915.
16. Kristiansen, N. I.; Stohl, A.; Olivié, D. J. L.; Croft, B.; Søvde, O. A.; Klein, H.; Christoudias, T.; Kunkel, D.; Leadbetter, S. J.; Lee, Y. H.; Zhang, K.; Tsigaridis, K.; Bergman, T.; Evangeliou, N.; Wang, H.; Ma, P. L.; Easter, R. C.; Rasch, P. J.; Liu, X.; Pitari, G.; Di Genova, G.; Zhao, S. Y.; Balkanski, Y.; Bauer, S. E.; Faluvegi, G. S.; Kokkola, H.; Martin, R. V.; Pierce, J. R.; Schulz, M.; Shindell, D.; Tost, H.; Zhang, H., Evaluation of observed and modelled aerosol lifetimes using radioactive tracers of opportunity and an ensemble of 19 global models. *Atmos. Chem. Phys.* **2016,** *16* (5), 3525-3561.
17. Zhang, H.; Ruehl, C. R.; Chan, A. W. H.; Nah, T.; Worton, D. R.; Isaacman, G.; Goldstein, A. H.; Wilson, K. R., OH-initiated heterogeneous oxidation of cholestane: A model system for understanding the photochemical aging of cyclic alkane aerosols. *J. Phys. Chem. A* **2013,** *117* (47), 12449-12458.
18. Renbaum, L. H.; Smith, G. D., Artifacts in measuring aerosol uptake kinetics: the roles of time, concentration and adsorption. *Atmos. Chem. Phys.* **2011,** *11* (14), 6881-6893.
19. Richards-Henderson, N. K.; Goldstein, A. H.; Wilson, K. R., Large Enhancement in the Heterogeneous Oxidation Rate of Organic Aerosols by Hydroxyl Radicals in the Presence of Nitric Oxide. *J. Phys. Chem. Lett.* **2015,** *6* (22), 4451-4455.
20. Chim, M. M.; Lim, C. Y.; Kroll, J. H.; Chan, M. N., Evolution in the Reactivity of Citric Acid toward Heterogeneous Oxidation by Gas-Phase OH Radicals. *ACS Earth Space Chem.* **2018,** *2* (12), 1323-1329.
21. Che, D. L.; Smith, J. D.; Leone, S. R.; Ahmed, M.; Wilson, K. R., Quantifying the reactive uptake of OH by organic aerosols in a continuous flow stirred tank reactor. *PCCP, Phys. chem. chem. phys. (Print)* **2009,** *11* (36), 7885-7895.
22. Richards-Henderson, N. K.; Goldstein, A. H.; Wilson, K. R., Sulfur Dioxide Accelerates the Heterogeneous Oxidation Rate of Organic Aerosol by Hydroxyl Radicals. *Environ. Sci. Technol.* **2016,** *50* (7), 3554-3561.
23. Zeng, M.; Heine, N.; Wilson, K. R., Evidence that Criegee intermediates drive autoxidation in unsaturated lipids. *Proceedings of the National Academy of Sciences* **2020,** *117* (9), 4486-4490.
24. Zhao, Z.; Yang, X.; Lee, J.; Tolentino, R.; Mayorga, R.; Zhang, W.; Zhang, H., Diverse Reactions in Highly Functionalized Organic Aerosols during Thermal Desorption. *ACS Earth Space Chem.* **2020,** *4* (2), 283-296.
25. Virtanen, A.; Joutsensaari, J.; Koop, T.; Kannosto, J.; Yli-Pirilä, P.; Leskinen, J.; Mäkelä, J. M.; Holopainen, J. K.; Pöschl, U.; Kulmala, M.; Worsnop, D. R.; Laaksonen, A., An

578 amorphous solid state of biogenic secondary organic aerosol particles. *Nature* **2010,** *467* (7317),
579 824-827.
580 26. Shiraiwa, M.; Li, Y.; Tsimpidi, A. P.; Karydis, V. A.; Berkemeier, T.; Pandis, S. N.;
581 Lelieveld, J.; Koop, T.; Pöschl, U., Global distribution of particle phase state in atmospheric
582 secondary organic aerosols. *Nature Communications* **2017,** *8* (1), 15002.
583 27. Zhao, Z.; Tolentino, R.; Lee, J.; Vuong, A.; Yang, X.; Zhang, H., Interfacial Dimerization
584 by Organic Radical Reactions during Heterogeneous Oxidative Aging of Oxygenated Organic
585 Aerosols. *J. Phys. Chem. A* **2019,** *123* (50), 10782-10792.
586 28. Zhao, Z.; Xu, Q.; Yang, X.; Zhang, H., Heterogeneous Ozonolysis of Endocyclic
587 Unsaturated Organic Aerosol Proxies: Implications for Criegee Intermediate Dynamics and Later-
588 Generation Reactions. *ACS Earth Space Chem.* **2019,** *3* (3), 344-356.
589 29. Zhao, Z.; Le, C.; Xu, Q.; Peng, W.; Jiang, H.; Lin, Y.-H.; Cocker, D. R.; Zhang, H.,
590 Compositional Evolution of Secondary Organic Aerosol as Temperature and Relative Humidity
591 Cycle in Atmospherically Relevant Ranges. *ACS Earth Space Chem.* **2019,** *3* (11), 2549-2558.
592 30. Zhao, Z.; Mayorga, R.; Lee, J.; Yang, X.; Tolentino, R.; Zhang, W.; Vuong, A.; Zhang,
593 H., Site-Specific Mechanisms in OH-Initiated Organic Aerosol Heterogeneous Oxidation
594 Revealed by Isomer-Resolved Molecular Characterization. *ACS Earth Space Chem.* **2020,** *4* (5),
595 783-794.
596 31. Zhao, Z.; Zhang, W.; Alexander, T.; Zhang, X.; Martin, D. B. C.; Zhang, H., Isolating
597 α-Pinene Ozonolysis Pathways Reveals New Insights into Peroxy Radical Chemistry and
598 Secondary Organic Aerosol Formation. *Environ. Sci. Technol.* **2021,** *55* (10), 6700-6709.
599 32. Mayorga, R. J.; Zhao, Z.; Zhang, H., Formation of secondary organic aerosol from nitrate
600 radical oxidation of phenolic VOCs: Implications for nitration mechanisms and brown carbon
601 formation. *Atmos. Environ.* **2021,** *244*, 117910.
602 33. Price, H. C.; Murray, B. J.; Mattsson, J.; O'Sullivan, D.; Wilson, T. W.; Baustian, K. J.;
603 Benning, L. G., Quantifying water diffusion in high-viscosity and glassy aqueous solutions using
604 a Raman isotope tracer method. *Atmos. Chem. Phys.* **2014,** *14* (8), 3817-3830.
605 34. Song, Y. C.; Haddrell, A. E.; Bzdek, B. R.; Reid, J. P.; Bannan, T.; Topping, D. O.;
606 Percival, C.; Cai, C., Measurements and Predictions of Binary Component Aerosol Particle
607 Viscosity. *J. Phys. Chem. A* **2016,** *120* (41), 8123-8137.
608 35. Yuan, B.; Koss, A. R.; Warneke, C.; Coggon, M.; Sekimoto, K.; de Gouw, J. A., Proton-
609 Transfer-Reaction Mass Spectrometry: Applications in Atmospheric Sciences. *Chem. Rev.* **2017,**
610 *117* (21), 13187-13229.
611 36. Zhang, X.; Krechmer, J. E.; Groessl, M.; Xu, W.; Graf, S.; Cubison, M.; Jayne, J. T.;
612 Jimenez, J. L.; Worsnop, D. R.; Canagaratna, M. R., A novel framework for molecular
613 characterization of atmospherically relevant organic compounds based on collision cross section
614 and mass-to-charge ratio. *Atmos. Chem. Phys.* **2016,** *16* (20), 12945-12959.
615 37. Krechmer, J. E.; Groessl, M.; Zhang, X.; Junninen, H.; Massoli, P.; Lambe, A. T.;
616 Kimmel, J. R.; Cubison, M. J.; Graf, S.; Lin, Y. H.; Budisulistiorini, S. H.; Zhang, H.; Surratt,
617 J. D.; Knochenmuss, R.; Jayne, J. T.; Worsnop, D. R.; Jimenez, J. L.; Canagaratna, M. R., Ion
618 mobility spectrometry–mass spectrometry (IMS–MS) for on- and offline analysis of atmospheric
619 gas and aerosol species. *Atmos. Meas. Tech.* **2016,** *9* (7), 3245-3262.
620 38. Butkovskaya, N. I.; Kukui, A.; Pouvesle, N.; Le Bras, G., Rate Constant and Mechanism
621 of the Reaction of OH Radicals with Acetic Acid in the Temperature Range of 229−300 K. *The*
622 *Journal of Physical Chemistry A* **2004,** *108* (34), 7021-7026.

39. Singleton, D. L.; Paraskevopoulos, G.; Irwin, R. S., Rates and mechanism of the reactions of hydroxyl radicals with acetic, deuterated acetic, and propionic acids in the gas phase. *Journal of the American Chemical Society* **1989,** *111* (14), 5248-5251.
40. Houle, F. A.; Hinsberg, W. D.; Wilson, K. R., Oxidation of a model alkane aerosol by OH radical: the emergent nature of reactive uptake. *Phys. Chem. Chem. Phys.* **2015,** *17* (6), 4412-4423.
41. Shiraiwa, M.; Pfrang, C.; Koop, T.; Pöschl, U., Kinetic multi-layer model of gas-particle interactions in aerosols and clouds (KM-GAP): linking condensation, evaporation and chemical reactions of organics, oxidants and water. *Atmos. Chem. Phys.* **2012,** *12* (5), 2777-2794.
42. Wiegel, A. A.; Liu, M. J.; Hinsberg, W. D.; Wilson, K. R.; Houle, F. A., Diffusive confinement of free radical intermediates in the OH radical oxidation of semisolid aerosols. *Phys Chem Chem Phys* **2017,** *19* (9), 6814-6830.
43. Slade, J. H.; Knopf, D. A., Multiphase OH oxidation kinetics of organic aerosol: The role of particle phase state and relative humidity. *Geophys. Res. Lett.* **2014,** *41* (14), 5297-5306.
44. Houle, F. A.; Wiegel, A. A.; Wilson, K. R., Changes in Reactivity as Chemistry Becomes Confined to an Interface. The Case of Free Radical Oxidation of C30H62 Alkane by OH. *J. Phys. Chem. Lett.* **2018,** *9* (5), 1053-1057.
45. Russell, G. A., Deuterium-isotope Effects in the Autoxidation of Aralkyl Hydrocarbons. Mechanism of the Interaction of PEroxy Radicals1. *J. Am. Chem. Soc.* **1957,** *79* (14), 3871-3877.
46. McNeill, V. F.; Yatavelli, R. L. N.; Thornton, J. A.; Stipe, C. B.; Landgrebe, O., Heterogeneous OH oxidation of palmitic acid in single component and internally mixed aerosol particles: vaporization and the role of particle phase. *Atmos. Chem. Phys.* **2008,** *8* (17), 5465-5476.
47. Lakey, P. S. J.; George, I. J.; Whalley, L. K.; Baeza-Romero, M. T.; Heard, D. E., Measurements of the HO2 Uptake Coefficients onto Single Component Organic Aerosols. *Environ. Sci. Technol.* **2015,** *49* (8), 4878-4885.
48. Liu, M. J.; Wiegel, A. A.; Wilson, K. R.; Houle, F. A., Aerosol Fragmentation Driven by Coupling of Acid–Base and Free-Radical Chemistry in the Heterogeneous Oxidation of Aqueous Citric Acid by OH Radicals. *J. Phys. Chem. A* **2017,** *121* (31), 5856-5870.
49. Smith, L. M.; Aitken, H. M.; Coote, M. L., The Fate of the Peroxyl Radical in Autoxidation: How Does Polymer Degradation Really Occur? *Accounts of Chemical Research* **2018,** *51* (9), 2006-2013.
50. Foret, M. K.; Lincoln, R.; Do Carmo, S.; Cuello, A. C.; Cosa, G., Connecting the "Dots": From Free Radical Lipid Autoxidation to Cell Pathology and Disease. *Chem. Rev.* **2020,** *120* (23), 12757-12787.
51. Helberg, J.; Pratt, D. A., Autoxidation vs. antioxidants – the fight for forever. *Chem. Soc. Rev.* **2021,** *50* (13), 7343-7358.
52. Ehn, M.; Thornton, J. A.; Kleist, E.; Sipila, M.; Junninen, H.; Pullinen, I.; Springer, M.; Rubach, F.; Tillmann, R.; Lee, B.; Lopez-Hilfiker, F.; Andres, S.; Acir, I.-H.; Rissanen, M.; Jokinen, T.; Schobesberger, S.; Kangasluoma, J.; Kontkanen, J.; Nieminen, T.; Kurten, T.; Nielsen, L. B.; Jorgensen, S.; Kjaergaard, H. G.; Canagaratna, M.; Maso, M. D.; Berndt, T.; Petaja, T.; Wahner, A.; Kerminen, V.-M.; Kulmala, M.; Worsnop, D. R.; Wildt, J.; Mentel, T. F., A large source of low-volatility secondary organic aerosol. *Nature* **2014,** *506* (7489), 476-479.
53. Denisov, E. T.; Afanas′ev, I. B., *Oxidation and antioxidants in organic chemistry and biology*. Taylor & Francis: Boca Raton, FL, 2005; p xxxviii, 981 p.
54. Bakker-Arkema, J. G.; Ziemann, P. J., Measurements of Kinetics and Equilibria for the Condensed Phase Reactions of Hydroperoxides with Carbonyls to Form Peroxyhemiacetals. *ACS Earth Space Chem.* **2020,** *4* (3), 467-475.

669 55. Maben, H. K.; Ziemann, P. J., Kinetics of oligomer-forming reactions involving the major
670 functional groups present in atmospheric secondary organic aerosol particles. *Environmental*
671 *Science: Processes & Impacts* **2023,** *25* (2), 214-228.
672 56. Krapf, M.; El Haddad, I.; Bruns, Emily A.; Molteni, U.; Daellenbach, Kaspar R.; Prévôt,
673 André S. H.; Baltensperger, U.; Dommen, J., Labile Peroxides in Secondary Organic Aerosol.
674 *Chem* **2016,** *1* (4), 603-616.
675 57. Pospisilova, V.; Lopez-Hilfiker, F. D.; Bell, D. M.; El Haddad, I.; Mohr, C.; Huang,
676 W.; Heikkinen, L.; Xiao, M.; Dommen, J.; Prevot, A. S. H.; Baltensperger, U.; Slowik, J. G.,
677 On the fate of oxygenated organic molecules in atmospheric aerosol particles. *Science Advances*
678 **2020,** *6* (11), eaax8922.
679 58. Mertes, P.; Pfaffenberger, L.; Dommen, J.; Kalberer, M.; Baltensperger, U., Development
680 of a sensitive long path absorption photometer to quantify peroxides in aerosol particles (Peroxide-
681 LOPAP). *Atmos. Meas. Tech.* **2012,** *5* (10), 2339-2348.
682 59. Pagonis, D.; Ziemann, P. J., Chemistry of hydroperoxycarbonyls in secondary organic
683 aerosol. *Aerosol Sci. Technol.* **2018,** *52* (10), 1178-1193.
684 60. Claflin, M. S.; Krechmer, J. E.; Hu, W.; Jimenez, J. L.; Ziemann, P. J., Functional Group
685 Composition of Secondary Organic Aerosol Formed from Ozonolysis of α-Pinene Under High
686 VOC and Autoxidation Conditions. *ACS Earth Space Chem.* **2018,** *2* (11), 1196–1210.
687 61. Crounse, J. D.; Nielsen, L. B.; Jørgensen, S.; Kjaergaard, H. G.; Wennberg, P. O.,
688 Autoxidation of organic compounds in the atmosphere. *J. Phys. Chem. Lett.* **2013,** *4* (20), 3513-
689 3520.
690 62. Atkinson, R., Atmospheric reactions of alkoxy and β-hydroxyalkoxy radicals. *Int. J. Chem.*
691 *Kinet.* **1997,** *29* (2), 99-111.
692 63. Che, D. L.; Smith, J. D.; Leone, S. R.; Ahmed, M.; Wilson, K. R., Quantifying the reactive
693 uptake of OH by organic aerosols in a continuous flow stirred tank reactor. *Phys. Chem. Chem.*
694 *Phys.* **2009,** *11* (36), 7885-7895.
695 64. Pöschl, U.; Shiraiwa, M., Multiphase Chemistry at the Atmosphere–Biosphere Interface
696 Influencing Climate and Public Health in the Anthropocene. *Chem. Rev.* **2015,** *115* (10), 4440-
697 4475.
698